

Restoration of Antibacterial Activity of Inactive Antibiotics via Combined Treatment with AgNPs

Nadia Ghaffar, Sumera Javad,* Anis Ali Shah, Saiqa Ilyas, Abeer Hashem, Graciela Dolores Avila-Quezada, Elsayed Fathi Abd_Allah, and Amina Tariq

Cite This: *ACS Omega* 2024, 9, 13621–13635

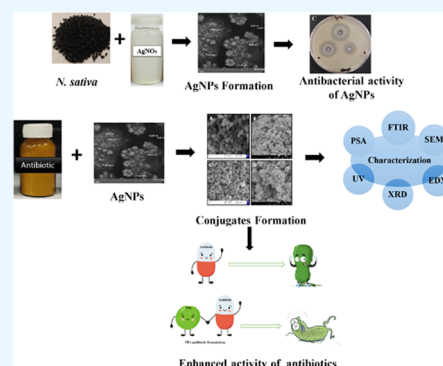
Read Online

ACCESS |

Metrics & More

Article Recommendations

ABSTRACT: Antimicrobial resistance poses a huge threat to human health around the world and calls for novel treatments. Combined formulations of NPs and antibiotics have emerged as a viable nanoplatform for combating bacterial resistance. The present research work was performed to investigate the effect of combined formulations of AgNPs with streptomycin, cefaclor, ciprofloxacin, and trimethoprim against multidrug-resistant (MDR) isolates of *Staphylococcus aureus* and *Klebsiella pneumoniae*. AgNPs have been synthesized by using the *Nigella sativa* seed extract, and their characteristics were analyzed. AgNPs depicted concentration-dependent antibacterial effects, as the highest concentration of AgNPs showed the strongest antibacterial activity. Interestingly, AgNPs in conjugation with antibiotics showed an enhanced antibacterial potential against both *S. aureus* and *K. pneumoniae*, which suggested synergism between the AgNPs and antibiotics. Against *S. aureus*, streptomycin and trimethoprim in conjugation with AgNPs presented a synergistic effect, while cefaclor and ciprofloxacin in combination with AgNPs showed an additive effect. However, all of the tested antibiotics depicted a synergistic effect against *K. pneumoniae*. The lowest value of MIC ($0.78 \mu\text{g/mL}$) was shown by AgNPs-Stp against *S. aureus*, whereas AgNPs-Tmp showed the lowest value of MIC ($1.56 \mu\text{g/mL}$) against *K. pneumoniae*. The most important point of the present study is that both organisms (*S. aureus* and *K. pneumoniae*) showed resistance to antibiotics but turned out to be highly susceptible when the same antibiotic was used in combination with AgNPs. These findings highlight the potential of nanoconjugates (the AgNPs-antibiotic complex) to mitigate the present-day crisis of antibiotic resistance and to combat antimicrobial infections efficiently.



1. INTRODUCTION

The prevalence of antimicrobial resistance is a worldwide challenge. Drug resistance is an inevitable and natural process that has been emerging for decades due to the overadministering and overutilization of antimicrobial drugs. It is a persistent health risk worldwide and one of the most common causes of death due to infectious diseases caused by these pathogenic bacteria.¹ Drug-resistant bacteria are affecting almost every person in the health sector by causing serious infections. In 2016, U.K. Government-commissioned Neil reported that it is critically needed to combat resistant bacterial infections. It is expected that infections caused by resistant organisms may be the main single cause of death for 10 million people per year by 2050.²

Staphylococcus aureus and *Klebsiella pneumoniae* are known to be the most common disease-causing human pathogens. They both cause sequelae of infections in all age groups, including both genders. *S. aureus* (a Gram-positive bacterium) causes many health problems. It may cause minor to severe skin infections and may become the cause of life-threatening issues. It causes osteomyelitis, abscess infection, sepsis, pneumonia, and

pseudomembrane enteritis.^{3,4} *S. aureus* is very difficult to treat because of the production of a biofilm, gliding mobility, staphyloxanthin pigment, and slime.^{5,6} According to Chambers and Deleo (2009), about 70–80% of *S. aureus* bacteria are methicillin-resistant, whereas about 90% are penicillin-resistant.⁷ *K. pneumoniae* is a Gram-negative bacterium. It is highly virulent and resistant to most antibiotics. It mostly becomes the cause of hospital-acquired infections and has worse effects on the lungs. It is the most prevalent pathogen and is responsible for many infections. *K. pneumoniae* contains a chromosomal β -lactamase gene, which naturally makes penicillins, such as ampicillin and amoxicillin, ineffective.^{8,9} Nowadays, there exists a huge burden of infectious diseases on the health of a living organism, the economy, and the community, and it is not

Received: September 13, 2023

Revised: February 15, 2024

Accepted: February 29, 2024

Published: March 14, 2024



possible to predict its worldwide cost.¹⁰ Existing antimicrobial treatments are now facing some drawbacks like their antagonistic interaction, restricted diversity, and overuse of antibiotics which is the major cause of resistance in microbes.¹¹

To increase and secure the health standards of the common man, new and efficient antibiotics are urgently needed to fight against resistant microbes. But it takes decades for the discovery, biosafety tests, and production of antibiotics for safe human use.¹² In this situation, enhancement of the antimicrobial potential of available antibiotics is a better option. In this area of research, nanotechnology is proving its strength. Silver nanoparticles (AgNPs) are economical, less toxic, and biosafe.^{13,14} AgNPs (even at lower concentrations)^{15–19} can inhibit the growth of many pathogenic bacterial strains.

The effect of nanoparticles on microorganisms varies because it depends upon the size and shape of NPs.^{20,21} The antibacterial activity of silver NPs is dependent on their shape. It is reported that round silver NPs are less active as compared to cubic AgNPs.^{22,23} The presence of vertexes and edges on the NP's surface facilitates the entrance of AgNPs into the microbial cell wall. Silver NPs have a larger surface area that provides more opportunity to cause stress to the microorganism and releasing more reactive oxygen species. Besides, the rate of resistance development in microorganisms toward AgNPs is much lesser.²⁴

The method to synthesize AgNPs is very simple, economical, facile, biocompatible, and environmentally friendly. For many biomedical applications, green synthesized nanoparticles have become a hot topic of research because of their ease of synthesis and low range of toxicity. In recent research, the combined effects of NPs (green synthesized) and forbidden antibiotics have been studied, and it has revolutionized the world. The antibacterial activity of antibiotics is increased against test bacteria when they are used in combination with NPs, as reported by many researchers, and it is supposed that nanoconjugates have the ability to reverse bacterial resistance.^{25–27} Nishanthi and co-workers (2019) reported that combined formulations of streptomycin-AgNPs showed enhanced antibacterial activity. They observed an 87.5% increase in the antimicrobial potential of streptomycin. They also reported a 100%-fold increase in the antibacterial potential of streptomycin in combination with gold nanoparticles.^{25,28}

Conjugates of antibiotics and silver nanoparticles may be considered an alternative to resistant bacterial strains because combined formulations of antibiotics-NPs not only reduce the dose of medicine but also minimize the chances of toxicity. Moreover, nanoconjugates exhibit a considerable enhancement in antibacterial activity in comparison to antibiotics alone. It is assumed that metal ions increase the membrane permeability by destabilizing the cell membrane. These metal ions also help the antibiotics to dodge bacterial cell immunity and gain entry into the cell. It is also reported that metal ions cause an enhancement of their efficiency inside the bacterial cell by penetrating more and accessing the target.²⁹

Consequently, research work was planned in an attempt to synthesize AgNPs by the green method using the aqueous extract of *Nigella sativa*. Characterization of the synthesized AgNPs was done by using different techniques to investigate their purity, morphology, size, and crystallinity. Antibiotics with different modes of action were selected for the synthesis of conjugates with AgNPs. The antibacterial potential of prepared AgNPs and the synergistic effect of antibiotics in conjugation with AgNPs were assessed against MDR *S. aureus* and *K. pneumoniae*. The present study aimed to check the effect of

antibiotics, in combination with AgNPs, against multidrug-resistant bacteria. It gives an understanding that conjugates can provide a ray of hope that antibiotics that are not in use today can be revived when combined with NPs. It can be a new horizon for treating fatal bacterial diseases in the agricultural, healthcare, and veterinary sectors.

2. EXPERIMENTAL SECTION

2.1. Materials. Seeds of *N. sativa* were purchased from the superstore, washed to remove the impurities, air-dried, and crushed, and then the powder was prepared by using an electric blender. To acquire uniform-sized particles, the seed powder was sieved through a mesh. The obtained powder was stored in an airtight jar for further analysis. The plant material collected and used was according to the institutional guidelines.

The purchase of silver nitrate (AgNO₃) and four antibiotics (streptomycin, cefaclor, ciprofloxacin, and trimethoprim) was made from Sigma-Aldrich. All of the purchased reagents were of analytical grade and used as received.

2.2. Pathogenic Strains. To investigate the antibacterial properties of AgNPs, *S. aureus* (Gram-positive bacteria) and *K. pneumoniae* (Gram-negative bacteria) (clinical isolate, pathogenic) were used as test organisms. Isolated microorganisms were studied using a microscope and a Vitek-2 system. To maintain the bacterial strains, nutrient agar with beef extract and sodium chloride were used. Before the experiment was started, nutrient broth was used to inoculate the bacterial strains to promote the growth of test organisms in the exponential phase.

2.3. Preparation of the Plant Extract. For extraction of the plant extract, plant material (50 g) was dissolved properly in distilled water (500 mL). The prepared mixture was added to closed vessels of a microwave-assisted extractor. Then, the vessels were adjusted in the extractor for the microwave-assisted extraction of plant material at 300 W of power level for 01 min. After completion of the MAE cycle, the obtained extract was filtered, and the filtrate was preserved at 4 °C for subsequent experimentation.³⁰

2.4. Phytochemical Analysis. The qualitative phytochemical analysis of *N. sativa* was carried out as per standard methods,^{31,32} which are summarized below.

2.4.1. Test for Phenolics. In 2 mL of the extract, a few drops of 5% FeCl₃·6H₂O solution were added, and a deep blue-black color showed the presence of phenolics.

2.4.2. Test for Flavonoids. In 2 mL of the extract, the addition of a few drops of ferric chloride hexahydrate (FeCl₃·6H₂O) showed an intense green color, which indicates the presence of flavonoids.

2.4.3. Test for Terpenoids. Two mL of chloroform was added to 5 mL of the plant extract, and then 3 mL of H₂SO₄ was added in it. At the interface of both chemicals, a reddish-brown coloration indicates the presence of terpenoids.

2.4.4. Test for Glycosides. One mL of the plant extract was diluted with 1 mL of water, and then 0.5 mL of lead acetate solution was added in it. Then, it was filtered and CHCl₃ was added and allowed to rest for some time. After evaporation of CHCl₃, 4–5 drops of ferric chloride, half mL of glacial acetic acid, and 2 mL of concentrated sulfuric acid were mixed with the test solution. The presence of glycosides was indicated by the appearance of two distinct layers in the test tube, a lower reddish-brown layer that changed to bluish-green and an upper acetic acid layer which remains the same.

2.4.5. Detection of Tannins. To detect tannins, the plant extract (1 mL) was diluted with 1 mL of water, and then, 2 to 3

drops of 10% ferric chloride were added in it. The appearance of brownish-green and bluish-black precipitates indicates a positive test for tannins.

2.4.6. Test for Saponins. For the detection of saponins, a total volume of 10 mL was prepared by diluting 0.5 mL of the plant extract with distilled water. The mixture was vigorously shaken for a minimum of 2 min. The occurrence of saponins was confirmed by the presence of creamy small bubbles like froth.

2.4.7. Test for Alkaloids. Concentrated hydrochloric acid (4 and 5 drops) was added to 1 mL of the plant extract. After stirring the reaction mixture carefully, it was treated with Dragendorff's reagent. The appearance of an orange color shows the presence of alkaloids.

2.5. Synthesis of Nanoparticles. For the green synthesis of AgNPs, 1, 2, and 3 mM aqueous solutions of AgNO₃ were prepared. Burets were filled with different concentrations of *N. sativa* extracts (10, 20, and 30 mg/mL). Silver nitrate solutions (10 mL) of different molarities were taken in beakers, and each concentration of the plant extract was added dropwise in all of the beakers containing prepared AgNO₃ solutions at 800 rpm by continuous stirring using a magnetic stirrer. Nine different types of AgNPs were prepared by adjusting the *N. sativa* extract ratio to the AgNO₃ solution (Table 1). The resultant mixture was

Table 1. Components of the Reaction Mixtures of Silver Nanoparticles with Their Abbreviations

AgNPs	conc. of AgNO ₃ (mM)	vol. of AgNO ₃ (mL)	vol. of <i>N. sativa</i> ext. (mL)	<i>N. sativa</i> NPs
sample A	1	10	10	AAGN ₁
			20	AAGN ₂
			30	AAGN ₃
sample B	2	10	10	BAGN ₁
			20	BAGN ₂
			30	BAGN ₃
sample C	3	10	10	CAGN ₁
			20	CAGN ₂
			30	CAGN ₃

centrifuged at 13,000 rpm for 15 min. Pallets were observed in the Eppendorfs tube, which were collected as mature AgNPs. Synthesized AgNPs were washed thrice with deionized water, dried in the air, and then stored carefully for further study.³³

2.6. Conjugation of Antibiotics with Nanoparticles. To prepare combined formulations of AgNPs and antibiotics, AgNPs with the smallest size were selected. Concentrations of antibiotics were used according to the CLSI standards. Phosphate buffer solution (1 mL) was taken in an Eppendorfs tube and 1 mg/mL AgNPs and antibiotics were added to it, mixed thoroughly, and incubated for 24 h. The resultant mixture was centrifuged at 10,000 rpm for 10 min. The supernatant was discarded, and conjugates of antibiotics-AgNPs were collected in the pallet form. Pallets were dried in air and then stored carefully to examine their activity.³⁴

2.7. Characterization of Silver Nanoparticles. Green synthesized AgNPs were characterized by using the following techniques.

2.7.1. UV–Vis Spectroscopy. An UV–vis spectrophotometer (BMS, UV-2600) was used to identify the reduction of metal ions. For this purpose, the wavelength was set from 200 to 700 nm and an aliquot of the reactant mixture was scanned between this range and data were recorded. It is an easily available and fast

technique that provides reliable information about the synthesis of NPs.³⁵

2.7.2. Particle Size Analysis (PSA). For the particle size analysis of AgNPs, a BT 90 nanolaser particle size analyzer was used. For PSA, 1 mg/mL AgNPs were dissolved in distilled water, sonicated properly, and subjected to a particle size analyzer for analysis. It provides data about the average particle sizes of NPs.³⁶

2.7.3. Scanning Electron Microscopy (SEM). To determine the surface morphology of green synthesized AgNPs, scanning electron microscopy was used. For this purpose, slides were prepared by forming a layer of AgNPs on the slides and then coating with a platinum layer for conductivity. Prepared slides were placed in the SEM at 20 kV voltage and model number (ZEISS-EVO/LS10) for micrographs. Data were recorded at different magnifications.³⁷

2.7.4. Energy-Dispersive X-ray (EDX) Analysis. The elemental composition of AgNPs and their qualitative and quantitative identification were done by using an EDX spectrometer attached with an SEM (ZEISS-EVO/LS10) at 20 kV voltage.³⁸

2.7.5. Fourier Transform Infrared Spectroscopic (FTIR) Analysis. FTIR data provide various modes of vibrations that are used to determine the presence of functional groups. For FTIR analysis, an IRT racer-100 FTIR spectrophotometer was used to obtain the spectrum. The sample was prepared by using AgNPs with KBr powder and the spectrum was taken in the range of 650–4000 cm⁻¹ at a resolution of 4 cm⁻¹.³⁹

2.7.6. X-ray Diffraction (XRD) Analysis. For XRD analysis, a Shimadzu XRD diffractometer (model 6000) containing a monochromator of graphite was utilized. It provided diffraction patterns with Cu-Kα radiation. A thin film of AgNPs was scanned at 2θ with 0.02° per step by attaining 5 s at each step. For the determination of crystalline phases, a standard powder diffraction card (Joint Committee on Powder Diffraction Standards-International Center for Diffraction Data) (JCPDS-ICSD) was utilized. The Scherrer equation was used to estimate the average crystallite size of AgNPs:

$$D = K\lambda/\beta \cos \theta$$

where *D* is the crystallite size (nm), *K* = 0.9 (Scherrer constant), λ = 0.15406 (X-ray wavelength), β is the full width at half-maximum (fwhm) of the diffraction peak, and θ is the peak position.⁴⁰

2.8. Evaluation of Antibacterial Activity. The agar well diffusion method is the most commonly used method to examine the antimicrobial activity of the NPs. In the present study, for the growth of bacterial strains, Muller–Hinton (MH) agar medium was used. The overnight-grown bacterial colony was used for the preparation of the bacterial suspension. A single colony was taken and dissolved in normal saline solution, and then its turbidity was adjusted to 0.5 McFarland standards. Bacterial strains were swabbed uniformly onto all of the prepared Petri plates by using sterile cotton swabs. Wells were prepared by using a gel puncture of 10 mm diameter on all of the prepared agar plates. AgNPs were dissolved in distilled water to prepare a 1 mg/mL solution. This solution was used to prepare further dilutions (100, 50, and 25 μg/mL). Wells were loaded with 100 μL of prepared solutions of AgNPs, AgNO₃ solution, and the *N. sativa* extract. The plate's position was not disturbed for 1 h to confirm the uniform diffusion of samples. Then, experimental plates were incubated overnight at 37 °C,

Table 2. Phytochemical Screening of Aqueous Extracts of *N. sativa*

<i>N. sativa</i> extract	secondary metabolites						
	phenolics	flavonoids	terpenoids	glycosides	tannins	saponins	alkaloids
aqueous MAE extract	++	+++	–	–	+	++	+++

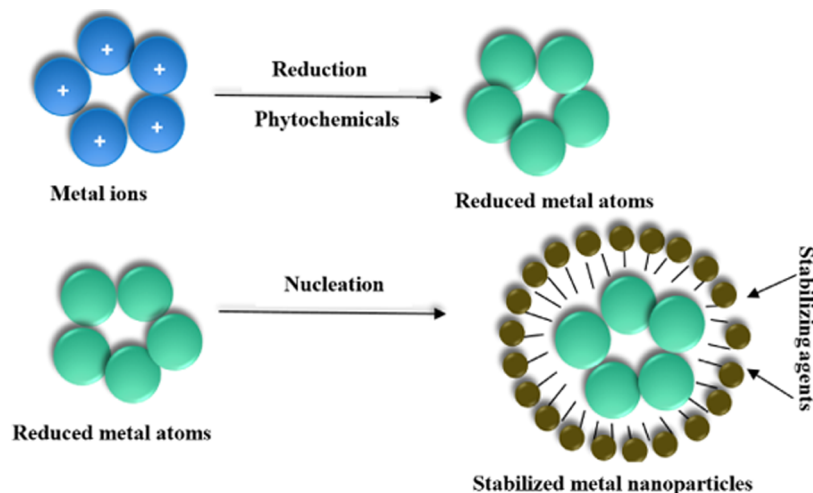


Figure 1. Schematic representation of the synthesis of metal nanoparticles.

inhibition zones (in mm) were measured, and data were recorded.³⁴

2.9. Determination of the Combined Effects of Antibiotics-AgNPs Formulations. To determine the combined effects of antibiotics-AgNPs, prepared conjugates (25 $\mu\text{g}/\text{mL}$) were loaded into the well, plates were not disturbed for a few minutes for even diffusion, and then they were placed in an incubator carefully at 35 $^{\circ}\text{C}$ for 24–48 h. For comparison, the antibacterial potential of AgNPs and antibiotics (streptomycin, cefaclor, ciprofloxacin, and trimethoprim) alone was also checked. The inhibition zones of AgNPs, antibiotics, and the antibiotics-AgNPs complex were measured in millimeters and compared to determine the enhancement in the activity of antibiotics.²⁵

2.10. Determination of the Minimum Inhibitory Concentration (MIC) of Antibiotics-AgNPs Formulations. The MIC of the combined formulations (the antibiotics-AgNPs complex) was determined by following the protocol of the Clinical Laboratory Standards Institute (CLSI) 2006. Conjugates were weighed accurately to prepare a 1 mg/mL solution. Fresh culture plates were prepared, isolated colonies (4–5) were taken from plates and added to the broth, and its turbidity was compared with the 0.5 MF (McFarland turbidity) standard (approximately 1.0×10^8 CFU/mL). By using broth, further dilutions (1:100 (10^6 CFU/mL)) can be made from the already prepared suspension. Test tubes were sterilized, and MH broth (1 mL) was poured into these tubes. The prepared experimental sample was added in tubes 1 and 2 and then serial dilutions were made to achieve particular concentrations of 12.5, 6.25, 3.12, 1.56, 0.78, and 0.39 $\mu\text{g}/\text{mL}$ and one extra tube was taken and set as a control. After that, tubes were inoculated with a freshly prepared bacterial suspension. Then, at 35–37 $^{\circ}\text{C}$ temperature, all of the prepared test tubes were incubated overnight. Growth of bacteria was examined visually and the minimum concentration of the conjugates which presented unmeasurable growth was considered the MIC.⁴¹

2.11. Evaluation of Fold Area Inhibition Measurement. By calculation of the mean surface area of the inhibition zone of each antibiotic, an increase in the fold area can be achieved. The following equation can be utilized to calculate the percentage of fold area inhibition for different antibiotics (streptomycin, cefaclor, ciprofloxacin, and trimethoprim).

$$\% \text{ fold increase} = \frac{(\text{AB} + \text{NPs}) - \text{AB alone}}{\text{AB alone}} \times 100$$

where AB is the inhibition zone by the antibiotic alone, and AB + NP is the inhibition zone by the antibiotic + green synthesized NPs.²⁵

2.12. Statistical Analysis. The significance of the data was analyzed by using SPSS software at the 5% level of significance. To compare the mean values of various parameters, one-way analysis of variance (ANOVA) was employed. Furthermore, Duncan's multiple range test was used as a post hoc test and for each measurement, three replicates were used.

3. RESULTS AND DISCUSSION

3.1. Phytochemical Analysis of *N. sativa*. Phytochemical analysis was performed to find out the phytochemicals present in the extract of *N. sativa*. This helps us to understand the phytochemicals involved in the green synthesis of silver nanoparticles. Extracts were analyzed for the presence of alkaloids, flavonoids, glycosides, phenolics, saponins, tannins, and terpenoids. Results showed that glycosides and terpenoids were absent from the black cumin seed extract, whereas the extract showed a significant amount of alkaloids and flavonoids. Other compounds were also present (Table 2).

It was observed that the *N. sativa* extract contains a reservoir of phytochemicals, and it can be linked to the results reported by Neel et al. (2023).⁴² It is also reported by many researchers that phytochemicals are the real key factors and have a reducing potential to synthesize and shape the NPs. So, the plant extracts with the best phytochemical profile play a significant role in the efficient production of NPs.⁴³

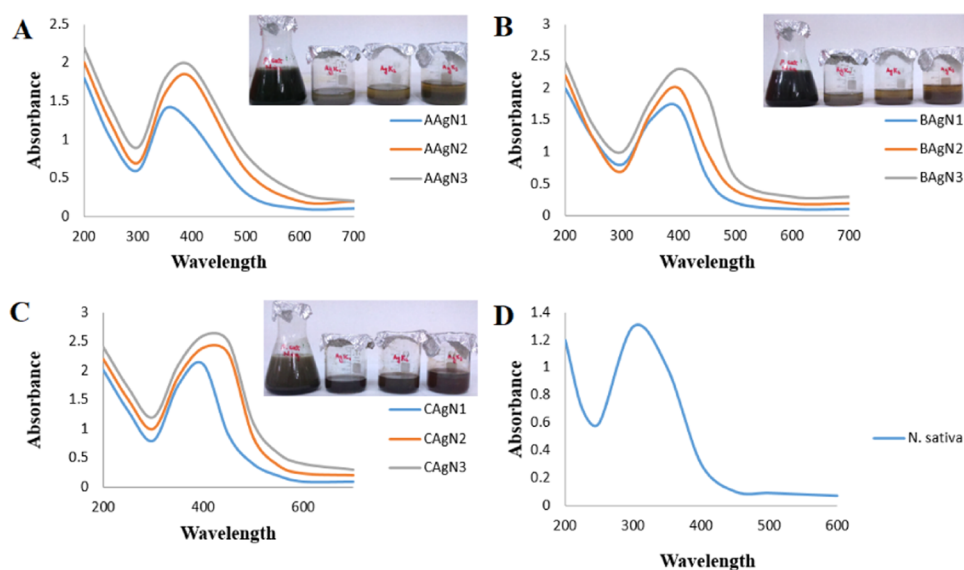


Figure 2. UV-vis spectra of biosynthesized AgNPs using various strengths of AgNO_3 : (A) 1 mM, (B) 2 mM, and (C) 3 mM. (D) Spectrum of the pure plant extract.

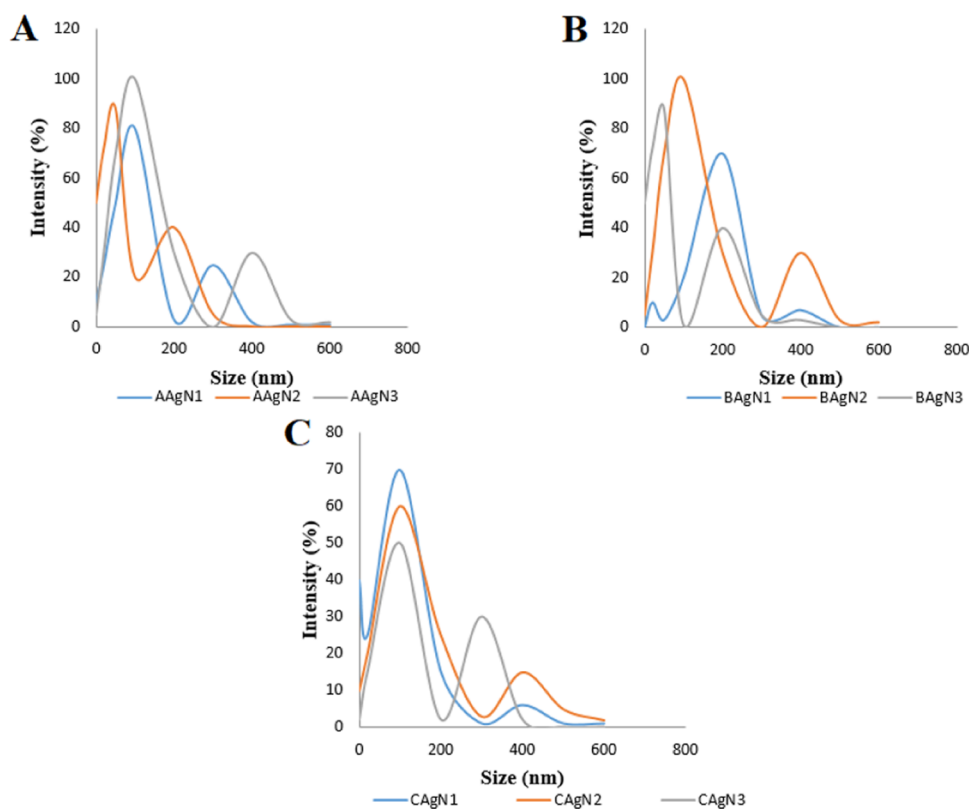


Figure 3. DLS measurements of the average size of biosynthesized AgNPs using various strengths of AgNO_3 : (A) 1 mM, (B) 2 mM, and (C) 3 mM.

3.2. Green Synthesis of Silver Nanoparticles. In the present research work, the effect of the aqueous *N. sativa* extract on the reduction of the metal precursor was evaluated. When an aqueous extract of *N. sativa* (10, 20, and 30 mg/mL) was poured by drops in a prepared solution (1, 2, and 3 mM) of AgNO_3 , a noticeable change in color was observed. Gradually, the color changed from olive green to dark green and finally to intense green, which points out the synthesis of AgNPs. By variation of the concentration of a salt solution with 10, 20, and 30 mg/mL *N. sativa* extract, a slight difference in color was observed. The

reaction mixture containing 2 mM AgNO_3 solution and the *N. sativa* extract (30 mg/mL) showed the maximum change in color (Figure 2A–D).

The plant extract-mediated synthesis of AgNPs by using the *N. sativa* extract as a stabilizing and reducing agent was primarily supported by color change. The change in color may occur due to the excitation of SPR vibrations in these NPs.⁴⁴ The phytochemicals of plants have a reducing potential that helps in the reduction of metal ions into metal NPs¹⁸ (Figure 1). The presence of phenolic compounds and the antioxidant activity of

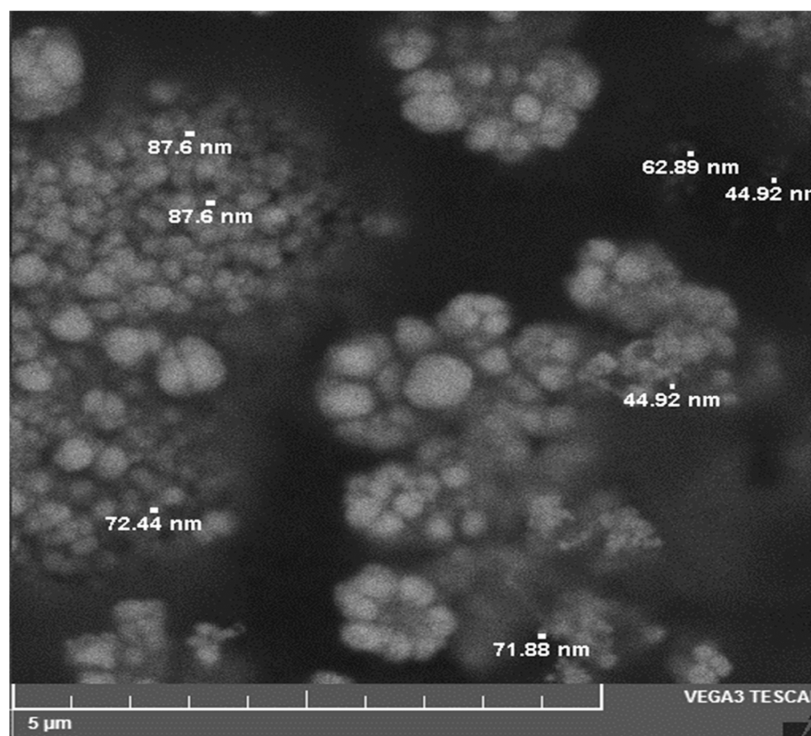


Figure 4. SEM micrograph of biosynthesized AgNPs.

N. sativa are already reported. The availability of H^+ ions is considered responsible for the reduction of silver ions into silver NPs.^{44–46} Visual detection of the formation of green synthesized nanoparticles with the metal precursor and the plant extract is also confirmed by many researchers.^{47,48}

3.3. UV–Visible Spectroscopy. Further, in the current study, the synthesis of AgNPs was monitored and confirmed through UV–visible spectroscopy, as it is one of the most convenient tools for measuring the reduction of metal ions based on optical properties. It provides us with information about the structure, size, aggregation, and stability of synthesized NPs. Because of the distinctive properties of AgNPs, they are dependent on concentration, refractive index, shape, and size. At the interface of AgNPs, surface plasmon resonance (SPR) is produced by the resonant oscillation of conduction electrons that were stimulated by the incident light. So, AgNPs showed characteristic optical absorption spectra in the UV–visible region. In our study, the UV–visible spectra of AgNPs (of samples A, B, and C) depicted single and strong maximum absorption peaks at 400, 420, and 430 nm, respectively, indicating the presence of isotropic and uniform-sized AgNPs (Figure 2A–D). Singh and Mijakovic (2022) also reported absorption peaks for AgNPs between 400–450 nm.³⁵

In this study, it was observed that by increasing the volume of the *N. sativa* extract, absorption peaks become sharper. It may be due to the presence of higher concentrations of metabolites in the *N. sativa* extract, which may play a considerable role in the capping and stabilization of AgNPs.⁴⁷ Interpretations of Selvaraj et al. (2019) are correlated with our findings.²⁹ Similar results were also presented by Amutha and Sridhar.⁴⁸

3.4. Particle Size Analysis. The size of the silver NPs was determined by using a nanolaser particle size analyzer, which is the most practical and fast technique. It can measure the average particle size distribution on both macro- and nanoscale. From PSA measurements, it was observed that silver nanoparticles of

various sizes were present in all reaction mixtures, but a higher percentage was found to be of small-sized AgNPs. The reaction mixture containing 2 mM $AgNO_3$ solution (10 mL) and the *N. sativa* seed extract (30 mL) presented the presence of the smallest-sized AgNPs in comparison to other treatments. It shows that the volume of the plant extract and the metal precursor concentration both are significant factors that can positively affect the size of AgNPs.^{36,49} It was assumed that up to a specific ratio of the metal precursor with the plant extract, a minimum size is retained, but a further change in both may form aggregates of the developed AgNPs due to which their size increases. PSA results indicate that by increasing the concentration of the metal precursor and the plant extract to a certain extent, a single peak is formed, which showed the uniform distribution of AgNPs, but a further increase in the concentration of the metal precursor causes an increase in the size of developed AgNPs due to aggregation^{50,51} (Figure 3A–C). In our research work, AgNPs ($BaAgN_3$) formed by using a prepared solution of the metal precursor (2 mM) and the *N. sativa* extract in a 1:3 ratio presented a minimum size, and so for further characterization and activity, this particular combination was utilized.

3.5. SEM Analysis. Surface morphology of the green synthesized AgNPs and their prepared conjugates with antibiotics was visualized by SEM analysis. From high-resolution SEM micrographs of silver NPs and conjugates, important data like size, topography, aggregation, shape, and their distribution were studied. The SEM image of AgNPs ($BaAgN_3$) is presented in Figure 4. Green synthesized silver NPs were studied by using a micron marker measuring 05 μm . The SEM micrograph depicted the presence of spherical, smooth-surfaced, and closely arranged AgNPs. It was seen that most of the NPs were individually arranged, but some aggregates were also observed, which most probably formed due to capping and stabilizing

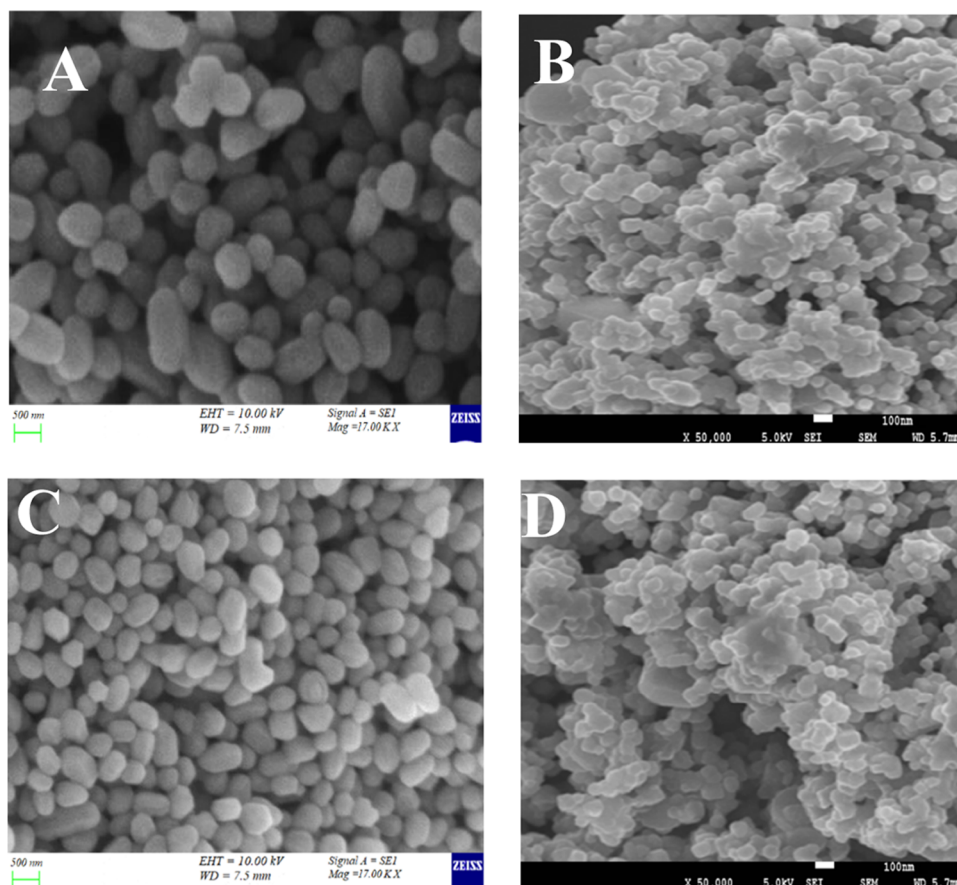


Figure 5. SEM micrographs showing combined formulations of AgNPs with (A) streptomycin, (B) cefaclor, (C) ciprofloxacin, and (D) trimethoprim.

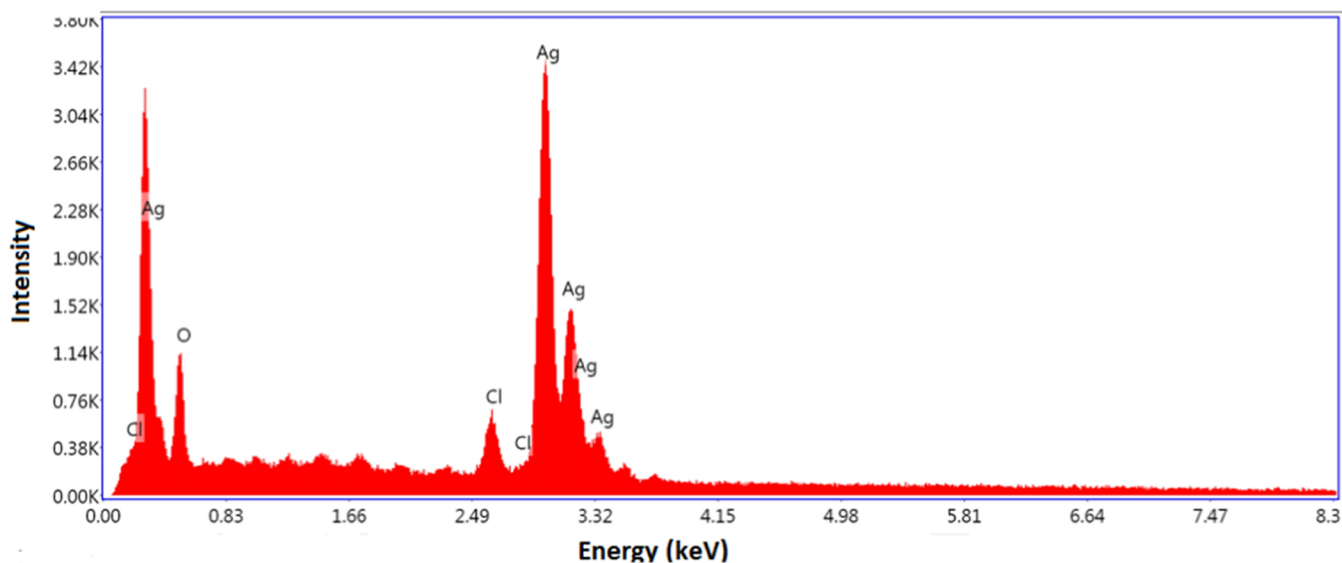


Figure 6. EDX spectrum of AgNPs (synthesized with 10 mL of AgNO_3 (2 mM) and 30 mL of the *N. sativa* extract).

agents present in the *N. sativa* seed extract. The estimated average size of silver nanoparticles was observed to be 67.46 nm.

SEM images of prepared conjugates of AgNPs with antibiotics are presented in Figure 5A–D. Streptomycin-AgNP conjugates were examined at a 500 nm micron marker. Their SEM images showed minimum aggregates with independently arranged particles. It was observed from the images that streptomycin-AgNP conjugates were spherical, oval, and hexagonal in shape

(Figure 5A). SEM micrographs of AgNPs-cefclor conjugates at a 100 nm micron marker identified a spherical and hexagonal shape. It was observed that conjugates were smooth on the surface and arranged closely with each other (Figure 5B). SEM images of AgNPs-Cpf at a 500 nm micron marker depicted the presence of a smooth-surfaced, spherical, and oval shape of the studied sample. In SEM images of AgNPs-Cpf, individually arranged conjugates of particular shapes were seen (Figure 5C).

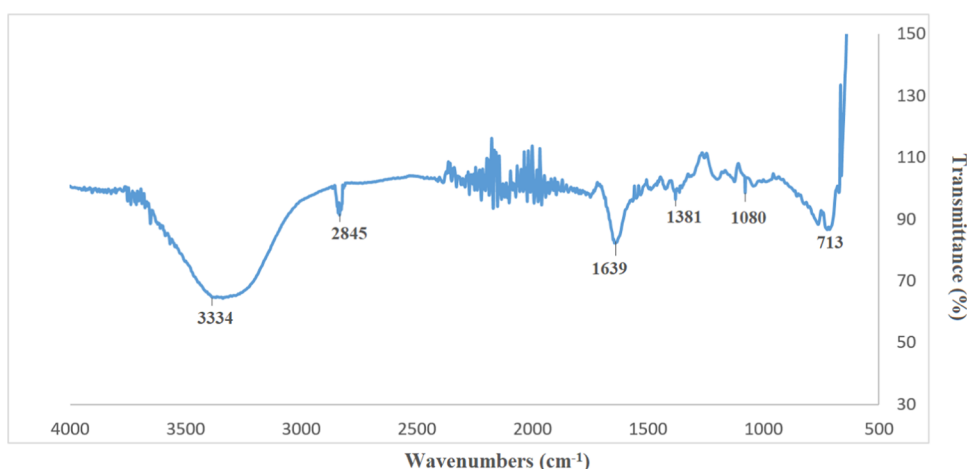


Figure 7. FTIR spectrum of the aqueous *N. sativa* seed extract.

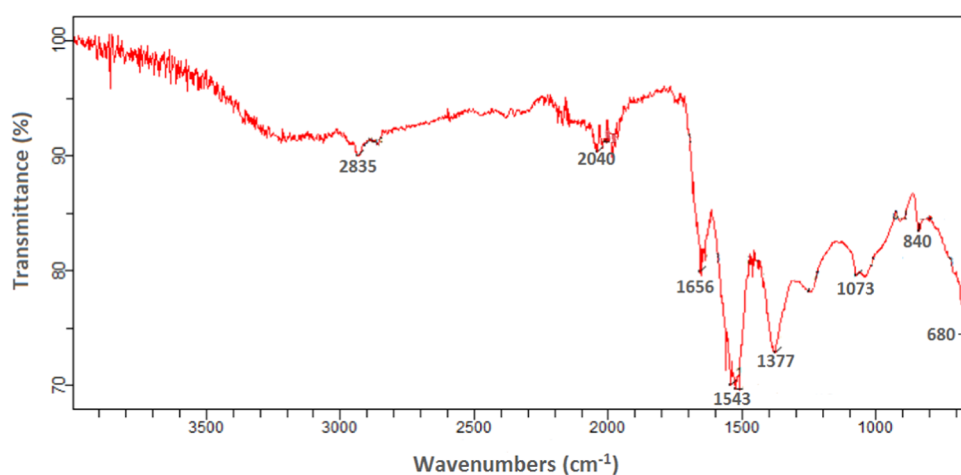


Figure 8. FTIR spectrum of AgNPs (synthesized with 10 mL of AgNO_3 (2 mM) and 30 mL of the *N. sativa* extract).

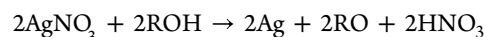
SEM images of AgNPs in conjugation with trimethoprim were examined at a 100 nm micron marker. Observations showed that most of the conjugates were hexagonal and spherical in shape and arranged much closer to each other (Figure SD).

According to the literature, it is reported that the type, concentration, and chemical composition of the plant extract significantly influence the size and shape of synthesized AgNPs. Nanoparticles synthesized by the green method may contain a thin layer of organic material (capping agent) due to which NPs attain stability. The size and shape of NPs are very important factors to study because they directly affect the properties of NPs. The antibacterial activity of AgNPs depends upon their size and shape, which determines the interaction of AgNPs with the microbe surface, which is considered responsible for their mode of action.³⁷

3.6. EDX Analysis. EDX analysis is used to determine the elemental mapping of green synthesized AgNPs. Figure 6 presents the EDX spectrum of silver NPs, exhibiting peaks corresponding to elemental silver (82.62%), as well as traces of chlorine and oxygen. Notably, a prominent peak at 3 keV further confirms the presence of silver. As it is reported in the literature that in the range 2.5–3.5 keV, AgNPs showed distinctive optical absorption peaks. EDX analysis showed that the silver peak may originate from silver NPs, while the appearance of other peaks showed the presence of the organic material of the plant extract. Our findings are similar to the study of Okaiyeto et al. (2019);

they performed the EDX analysis of green synthesized silver NPs, determined their elemental composition, and showed related results.³⁸

3.7. FTIR Spectroscopy. FTIR analysis was employed to examine the functional groups that are responsible for the capping, reduction, and stability of the green synthesized AgNPs. Spectral peaks for the aqueous *N. sativa* seed extract were detected at 3334, 2845, 1639, 1381, 1080, and 713 cm^{-1} (Figure 7), whereas the FTIR spectrum of synthesized AgNPs using the *N. sativa* seed extract showed the presence of vibrational frequencies at 2835, 1656, 1377, 1073, 840, and 680 cm^{-1} (Figure 8). The appearance of a peak at 3334 cm^{-1} of the *N. sativa* extract depicted the existence of an –OH group, which corresponds to phenolic compounds.⁵² Therefore, the hydroxyl functional group (–OH) is believed to be responsible for the reduction of silver ions (Ag^+) into metallic silver (Ag) through alcoholic oxidation (R-OH), leading to the formation of an aldehyde group (R=O), as depicted in the following equation:



It shows that the presence of phenolic compounds in the *N. sativa* seed extract is of considerable importance because they act as reducing and stabilizing agents during the synthesis of AgNPs.⁵³ The appearance of the *N. sativa* extract peak at 2845 cm^{-1} was shifted to a low-frequency peak at 2835 cm^{-1} in the AgNP spectra, which corresponded to the C–H stretch of

alkanes. Moreover, peaks observed in the range of 2500–2000 cm^{-1} indicate the presence of vibrations related to $\text{C}\equiv\text{C}$ and $\text{C}\equiv\text{N}$ functional groups. The peak of the *N. sativa* extract that appears at 1635 cm^{-1} and the band of AgNPs noticed at 1656 cm^{-1} were attributed to the presence of the carbonyl functional group $\text{C}=\text{O}$. The appearance of peaks between 1073 and 1377 cm^{-1} corresponded to $\text{C}-\text{O}$ and $\text{CO}=\text{C}-\text{OC}$ stretching vibrations of alcohols and esters. Additionally, the peak detected at 1080 cm^{-1} of the *N. sativa* extract was moved to 1073 cm^{-1} in the developed silver NPs, indicating the presence of $\text{C}-\text{O}$ stretching vibrations, and this shift confirms the presence of flavonoids on the surface of silver NPs.^{39,54} The peaks observed at 680 and 840 cm^{-1} are linked to the $\text{C}-\text{H}$ stretching vibrations of aromatic compounds and amines. The bands of organic compounds were mostly observed in the functional group region, while the appearance of absorption bands in the fingerprint region showed the presence of metals. FTIR measurements depicted the effect of functional groups in the capping and stabilization of NPs.

3.8. XRD Analysis. XRD (X-ray diffraction) analysis provides information about the crystalline nature of the green synthesized silver NPs. Figure 9 presents the XRD pattern of

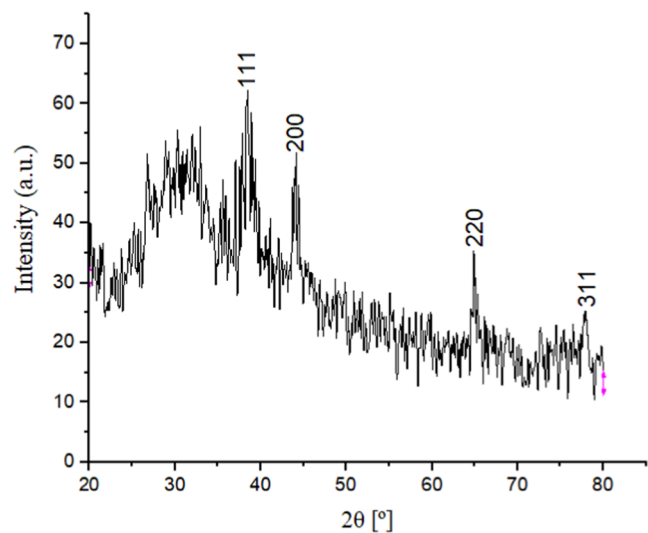


Figure 9. XRD spectrum of AgNPs (synthesized with 10 mL of AgNO_3 (2 mM) and 30 mL of the *N. sativa* extract).

green synthesized AgNPs. For XRD analysis, the dried powder of AgNPs was subjected to an analyzer, and four diffraction peaks were observed at 2θ of 38.50, 44.13, 64.91, and 77.89° corresponding to (111), (200), (220), and (311) silver crystal

planes, respectively (Figure 9). The appearance of diffraction peaks confirmed that AgNPs exhibited a face-centered cubic (FCC) lattice structure, which is consistent with the standard powder diffraction card (JCPDS) No. 04–0783. Our results are in accordance with the findings of Al-Aboody (2019), who reported the face-centered cubic (FCC) lattice structure of silver nanoparticles with similar crystal planes.⁴⁰

The measured average crystallite size of the biosynthesized AgNPs was 3.1 nm. The XRD spectrum showed some other peaks as well other than silver nanocrystals, which might originate from the organic material found in the plant extract.

3.9. Antibacterial Activity of Green Synthesized AgNPs. In the present research work, the antibacterial potential of green synthesized NPs was determined against *S. aureus* and *K. pneumoniae* by the agar well diffusion method. The *N. sativa* seed extract, AgNO_3 solution, and AgNPs were examined for their antibacterial activity. AgNPs presented a prominent clear inhibition zone in comparison to the *N. sativa* seed extract and AgNO_3 solution, which confirmed the effectiveness of AgNPs, as seen in Figure 10.

The Gram-positive bacteria, *S. aureus*, exhibited a much higher sensitivity to AgNPs in comparison to *K. pneumoniae* (Gram-negative bacteria). The maximum activity measured against *S. aureus* was 23 ± 0.5 mm at a concentration of 100 $\mu\text{g}/\text{mL}$, while the inhibition zone of AgNPs recorded against *K. pneumoniae* was 09 ± 0.7 mm (Figure 10A,B). Our results are significantly better than Hussein et al. (2019); they also reported the antibacterial activity of green synthesized AgNPs.⁵⁵

The effectiveness of AgNPs was found to be higher against Gram-positive bacteria. AgNPs have the ability to damage the cell membrane of both Gram-positive bacteria such as *S. aureus* and Gram-negative bacteria such as *K. pneumoniae*, but the difference in activity of AgNPs for both organisms may appear due to modifications in the composition of the bacterial cell wall and the AgNP interaction with the cell wall of the bacteria.

Khorrami et al. (2018) reported that silver NPs produce Ag^+ , which is attached to the cell wall and the cytoplasmic membrane of organisms due to which the permeability of the cytoplasmic membrane increases, leading to the disruption of the bacterial envelope.⁵⁶ Movement of Ag^+ into the bacteria produces reactive oxygen species (ROS) by deactivating respiratory enzymes and causes an interruption in the generation of adenosine triphosphate. ROS production initiates the cell membrane damage and causes alteration in deoxyribonucleic acid (DNA). When silver ions come in contact with essential components (phosphorus and sulfur) of DNA, they interrupt the replication process of DNA, leading to the termination of reproduction and ultimately cell death. Moreover, silver ions can inhibit protein synthesis by denaturing the ribosomes found in

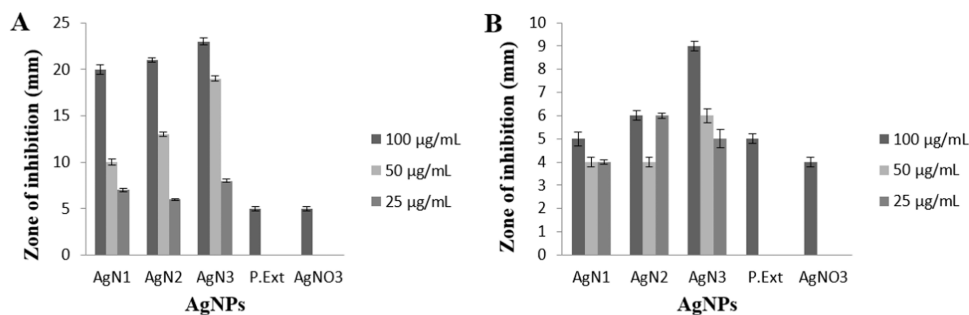


Figure 10. Antibacterial activity of AgNPs against (A) *S. aureus* and (B) *K. pneumoniae*.

Table 3. Antibacterial Potential of Antibiotics Alone and in Synergy with Biosynthesized Silver Nanoparticles against *S. aureus*^a

antibiotics	inhibition zones in mm			
	antibiotics alone (a)	AgNPs alone (25 μg/mL)	AB + AgNPs (b)	%-fold increase = $((b - a)/a) \times 100$
streptomycin	00 ± 0.0 ^a	08 ± 0.7	13 ± 0.5	130
cefaclor	03 ± 0.7	08 ± 0.7	13 ± 0.2	333
ciprofloxacin	12 ± 0.5	08 ± 0.7	28 ± 0.5	133
trimethoprim	00 ± 0.0 ^a	08 ± 0.7	12 ± 0.5	120

^aIn the absence of bacterial growth inhibition zones, the disc diameter (6 mm) was used to calculate the fold increase.

Table 4. Antibacterial Potential of Antibiotics Alone and in Synergy with Biosynthesized Silver Nanoparticles against *K. pneumoniae*^a

antibiotics	inhibition zones in mm			
	antibiotics alone (a)	AgNPs alone (25 μg/mL)	AB + AgNPs (b)	%-fold increase = $((b - a)/a) \times 100$
streptomycin	00 ± 0.0 ^a	5 ± 0.5	11 ± 0.4	110
cefaclor	00 ± 0.0 ^a	5 ± 0.5	12 ± 0.2	120
ciprofloxacin	00 ± 0.0 ^a	5 ± 0.5	15 ± 0.5	150
trimethoprim	00 ± 0.0 ^a	5 ± 0.5	24 ± 0.2	240

^aIn the absence of bacterial growth inhibition zones, the disc diameter (6 mm) was used to calculate the fold increase.

the cytoplasm.⁵⁷ Furthermore, Ag⁺ can modify the three-dimensional structure of synthesized proteins by blocking their active sites and hindering the overall functioning of the microorganism.^{58,59}

Apart from releasing Ag⁺, AgNPs themselves have the capability to terminate the growth of microorganisms. Nano-sized silver NPs can enter into the bacterial cell wall more actively and cause cell membrane damage due to the instability of two layers of lipid molecules caused by ROS (reactive oxygen species) generation. The excess ROS production disturbs redox homeostasis, leading to oxidative stress.⁶⁰ Many reactive oxygen species such as OH⁻ (hydroxyl ion), O₂⁻ (superoxide anion), and H₂O₂ (hydrogen peroxide) are considered responsible for toxic effects. Usually, H₂O₂ permeates into the bacterial cell wall and then into a cell membrane, interacts with bacterial DNA, lipids, and proteins, and causes the misconfiguration of ion channels by damaging transporter proteins. It damages DNA and RNA and causes their fragmentation. It inhibits the catalytic domains of enzymes and interrupts their physiology. Denaturation of proteins and damage to biomolecules ultimately cause cell lysis.^{61,62}

In our study, it was evaluated that AgNPs developed by using 30 mL of the *N. sativa* extract with 10 mL of silver nitrate solution (2 mM) presented the highest antibacterial activity (Figure 8A,B). From the results, it was concluded that synthesis conditions of AgNPs have a considerable effect on their efficiency, like the adequate amount of AgNO₃ (silver nitrate) and stabilizing agents derived from *N. sativa* facilitate in the production of AgNPs with smaller particle sizes, which ultimately affect its antibacterial potential and become the best possible reason for the effectiveness of smaller-sized AgNPs.⁶³

Further, it was noticed that green synthesized AgNPs depicted a dose-dependent activity (at higher doses, the recorded inhibitory action was higher). AgNPs showed the maximum activity at a final dose of 100 μg/mL; by decreasing the dose from 50 to 25 μg/mL, a prominent decrease in the activity of AgNPs was observed (Figure 10A,B). The shape, size, and dose of AgNPs have a considerable effect on their antibacterial activity.⁵⁶ Small NPs have a large surface-to-volume ratio that assists AgNPs in their interaction with bacteria, leading to

enhanced biological activity. AgNPs also cause a dose-dependent increase in oxidation and DNA damage.⁶⁴

3.10. Evaluation of the Synergistic Effect of Antibiotics with AgNPs against Pathogenic Bacteria. The synergistic effect of antibiotics in combination with AgNPs was investigated against *S. aureus* and *K. pneumoniae* and the question whether combining AgNPs with antibiotics enhances the antibacterial activity of antibiotics or not was also addressed in this study and found true (Tables 3 and 4). Tables 3 and 4 present the antibacterial activity of antibiotics alone and their conjugates with biosynthesized AgNPs against *S. aureus* and *K. pneumoniae*. Results concluded that AgNPs and antibiotics showed very minute or no activity, while their combined treatment showed a significantly enhanced antibacterial activity, which showed a positive effect of their combination. Interestingly, the inactive antibiotic also becomes active against bacteria when used in combination with AgNPs. Figures 11B–E and 12B–E also present the prominent inhibition zones around the well containing the combined formulation of AgNPs and antibiotics.

S. aureus (a Gram-positive bacterium) was observed to be sensitive to cefaclor and ciprofloxacin and showed resistance toward streptomycin and trimethoprim (Figure 11B–E), whereas *K. pneumoniae* (a Gram-negative bacterium) was found resistant toward all of the selected antibiotics (streptomycin, cefaclor, ciprofloxacin, and trimethoprim) (Figure 12B–E). Against *S. aureus*, a maximum synergistic effect was presented by a combined formulation of the AgNPs-streptomycin complex, while against *K. pneumoniae*, AgNPs-trimethoprim conjugates showed the highest enhanced antibacterial activity (Figures 11B and 12E). It was observed that all of the plates, well inoculated with conjugates, depicted significantly higher inhibition zones in comparison to AgNPs and antibiotics alone, which confirmed the enhancement in the activity of antibiotics. Against *S. aureus*, AgNPs-Stp showed a 130%-fold increase, whereas against *K. pneumoniae*, AgNPs-Tmp depicted a 240%-fold increase in antibacterial activity (Figures 11A and 12A). Specific interactions of conjugates with the cell membrane of bacteria due to bonding reactions between AgNPs and antibiotics cause the enhanced antibacterial potential of antibiotics.⁶⁵ Nanoparticles ensure the slower but increased release of antibiotics from their surface, thus ensuring

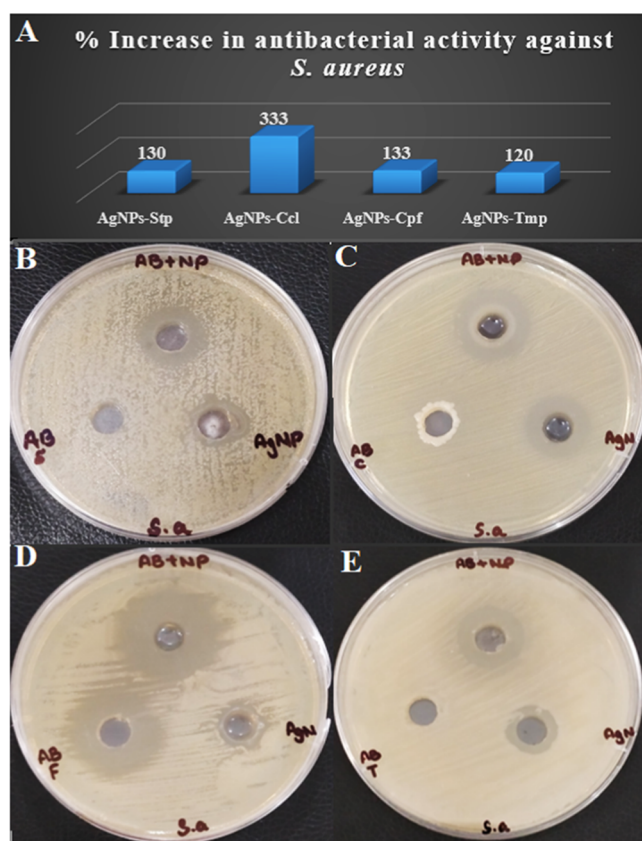


Figure 11. Synergistic effect of antibiotics with silver NPs: (A) percent increase in the antibacterial activity of antibiotics in combination with silver nanoparticles (B) AgNPs-Stp, (C) AgNPs-Ccl, (D) AgNPs-Cpf, and (E) AgNPs-Tmp against *S. aureus*. AB + NP: antibiotic loaded with NPs, ABS: antibiotic streptomycin, ABC: antibiotic cefaclor, ABF: antibiotic ciprofloxacin, ABT: antibiotic trimethoprim, AgN: silver NPs of *N. sativa*, and S.a: *S. aureus*. AgNPs-Stp (combined formulation of AgNPs and streptomycin), AgNPs-Ccl (combined formulation of AgNPs and cefaclor), AgNPs-Cpf (combined formulation of AgNPs and ciprofloxacin), and AgNPs-Tmp (combined formulation of AgNPs and trimethoprim).

their longer life and action time. Silver nanoparticles themselves have a strong antibacterial activity that is dependent upon their shape and size. Therefore, when silver nanoparticles are combined with nanoparticles in conjugates, they have enhanced antibacterial activity against Gram-negative as well as Gram-positive bacteria.⁶⁶

From the results, it was observed that against *S. aureus*, AgNPs in combination with streptomycin and trimethoprim showed a synergistic effect, and cefaclor and ciprofloxacin presented an additive effect. However, AgNPs in conjugation with all of the selected antibiotics showed a synergistic effect against *K. pneumoniae*.

3.11. Minimum Inhibitory Concentration (MIC) of Antibiotics-AgNPs Formulations against *S. aureus* and *K. pneumoniae*. The MIC of silver NPs-antibiotics combination (AgNPs-Stp, AgNPs-Ccl, AgNPs-Cpf, and AgNPs-Tmp) was evaluated against *S. aureus* and *K. pneumoniae* after confirmation of their antibacterial activity. The MIC of AgNPs-Stp, AgNPs-Ccl, AgNPs-Cpf, and AgNPs-Tmp against both organisms is presented in the table below (Table 5). From the results, it was observed that AgNPs-Stp showed the lowest value of MIC (0.78) against *S. aureus* and AgNPs-Tmp showed

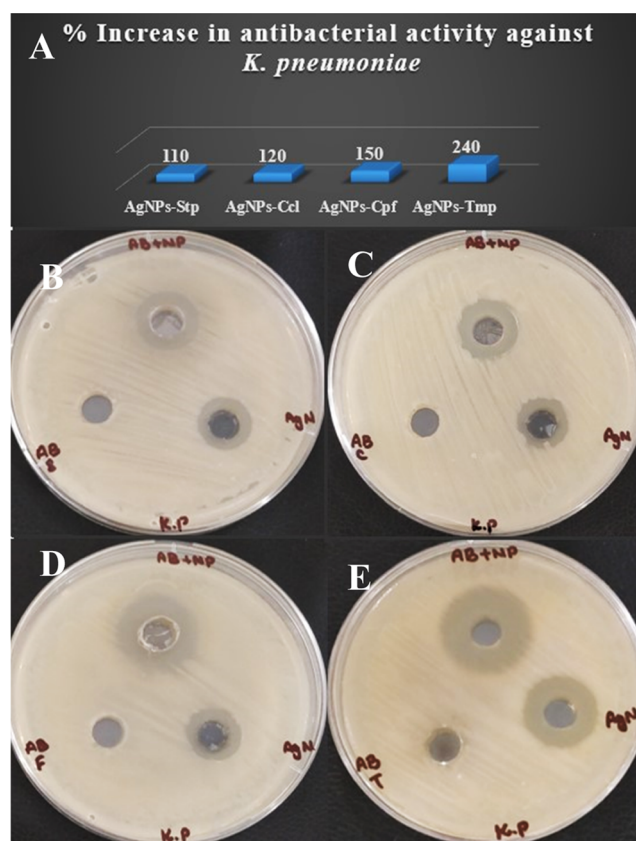


Figure 12. Synergistic effect of antibiotics with silver NPs: (A) percent increase in the antibacterial activity of antibiotics in combination with silver nanoparticles (B) AgNPs-Stp, (C) AgNPs-Ccl, (D) AgNPs-Cpf, and (E) AgNPs-Tmp against *K. pneumoniae*. AB + NP: antibiotic loaded with NPs, ABS: antibiotic streptomycin, ABC: antibiotic cefaclor, ABF: antibiotic ciprofloxacin, ABT: antibiotic trimethoprim, AgN: silver NPs of *N. sativa*, and K.p: *K. pneumoniae*. AgNPs-Stp (combined formulation of AgNPs and streptomycin), AgNPs-Ccl (combined formulation of AgNPs and cefaclor), AgNPs-Cpf (combined formulation of AgNPs and ciprofloxacin), and AgNPs-Tmp (combined formulation of AgNPs and trimethoprim).

Table 5. Evaluation of the Minimum Inhibitory Concentration ($\mu\text{g/mL}$) of Prepared Conjugates against *S. aureus* and *K. pneumoniae*^a

s. no	conjugates of AgNPs	MIC of conjugates ($\mu\text{g/mL}$) ^a	
		<i>S. aureus</i>	<i>K. pneumoniae</i>
1	AgNPs-Stp	0.78	6.25
2	AgNPs-Ccl	1.56	3.12
3	AgNPs-Cpf	1.56	3.12
4	AgNPs-Tmp	3.12	1.56

^aResults showed the mean of three different experiments. Standard deviations did not exceed 5%. Concentration is expressed in $\mu\text{g/mL}$.

the lowest value of MIC (1.56) against *K. pneumoniae* (Figure 13).

There is no exact known mechanism of conjugate formation (the NPs-antibiotics complex) but there are two assumptions.^{67,68}

First, it is supposed that the greater surface-area-to-volume ratio of the nanomaterial helps in conjugate formation by interacting with the antibiotic molecule that leads to binding of the antibiotic to the penicillin-binding protein (PBP) membrane-associated protein receptor. It assists in the accumulation

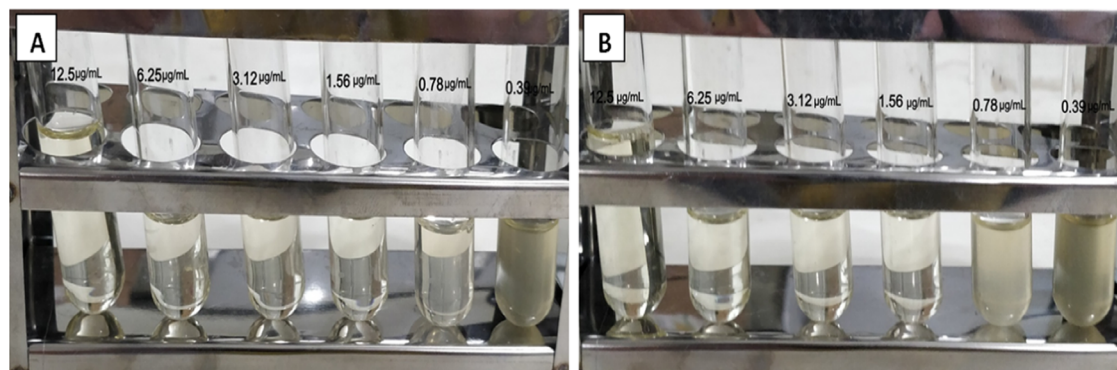


Figure 13. MIC of (A) AgNPs-Stp against *S. aureus* and (B) AgNPs-Tmp against *K. pneumoniae*.

of the antibiotic molecule on the outer surface of the microorganism's membrane.⁶⁷ It weakens the osmotic balance due to which the cell membrane damages and the cell wall synthesis of bacteria is inhibited. The cytoplasmic content leaks out, leading to bacterial cell death.⁶⁹

Second, the conjugates (the antibiotic-NPs complex) not only bind and penetrate the bacterial cell wall but also target many other sites.⁷⁰ The movement of conjugates inside the cell causes disturbance in the regulatory functions, disrupts the formation of bioactive proteins, disables the interaction between sulfur-phosphorus and DNA, and totally inhibits protein synthesis.⁶⁷

Most of the available antibiotics are not able to reach high intracellular concentrations because of transport scarcity. In the existence of resistance mechanisms, this situation becomes worse, such as a decreased uptake of antibiotics and increased efflux. The high surface-area-to-volume ratio of AgNPs is a considerable factor in its effectiveness. Surface forces become more prominent when there is an increased surface-area-to-volume ratio, primarily due to a higher percentage of atoms at the surface. It helps in the binding of AgNPs to the proteins of the bacterial cell membrane, leading to increased permeability due to which the infiltration of antibiotics into the bacterial cell also increases. Consequently, AgNPs in combination with antibiotics increase the concentration of antibiotics at a definite point on the cell membrane.^{71,72}

AgNPs can attach to the surface of the bacterial cell due to electrostatic attraction between the positive surface charge of AgNPs and the negatively charged cell membrane. In the bacterial cell wall, some sulfur-containing proteins interact with silver ions and damage the cell wall of bacteria.⁷³ The nanosize of AgNPs assists in the interaction with the bacterial envelope and the cell membrane and can easily inhibit the crucial metabolic pathways.⁷⁴

Li and co-workers (2005) studied AgNPs-amoxicillin synergistic properties. They explain that in conjugates of amoxicillin-AgNPs, many molecules of amoxicillin surround each silver nanoparticle, positioning themselves between the $-OH$ (hydroxyl) and $-NH_2$ (amino) groups of amoxicillin.⁷⁵ Duran et al. (2010) reported the binding between AgNPs and amoxicillin by a sulfur bridge. It influences its penetration and effectiveness inside the bacteria.⁷⁶ Multiple researchers have reported that localizing the antibiotics on the bacterial surface enhances the drug-bacteria interaction due to which binding of the organism and the drug leads to blockage of bacterial efflux pumps and enhances the antibacterial effect of the conjugate.^{70,77,78}

In 2015, Roshmi and co-workers studied gold nanoparticles (AuNPs); they reported that antibiotics can attach to the surface of AuNPs by electrostatic attraction and can be used as a carrier for antibiotics.⁷⁹ Magalhaes and Mosqueira (2010) studied that poorly water-soluble antibiotics in combination with AuNPs showed better solubility. The AuNPs-antibiotic complex enhances the drug release and improves the half-life of the drug.^{80,81} Kamal et al. also reported the enhanced drug loading capacity of nanofibers when used with cephalexin against multidrug-resistant *S. aureus*.⁸²

From the results, it was concluded that AgNPs interrupt the bacterial cell wall and allow antibiotic access into the bacterial cell. Combined formulations of AgNPs-antibiotics, at a particular site of the cell membrane, enhance the quantity of antibiotics that primarily disturbed the essential metabolic pathways that led to harm to the protein-synthesizing machinery, which ultimately causes cell lysis. Combined treatment of antibiotics-AgNPs facilitates the usage of those antibiotics that are now not in use because of resistant bacteria. It provides possibilities for the treatment of bacterial diseases in the healthcare, agricultural, and veterinary sector. To combat multidrug-resistant bacteria, further research is still an urgent need in our society to develop more efficient and feasible designs for the development of new and novel antimicrobial agents and drugs.

4. CONCLUSIONS

The utilized green method in this investigation provides spherical AgNPs with an average diameter of 67.46 nm with high crystallinity. An excellent agreement between the particle size measurements was observed using different techniques. AgNPs in conjugation with antibiotics showed an enhanced antibacterial potential against both Gram-positive (*S. aureus*) and Gram-negative (*K. pneumoniae*) bacteria. Combined treatment of AgNPs with antibiotics presented the maximum synergistic effect against *S. aureus*. Both organisms *S. aureus* and *K. pneumoniae* showed resistance to antibiotics but became susceptible when the same antibiotic was utilized in conjugation with AgNPs. The combined action of antibiotics with silver NPs opens an alternative area of research aimed at combating drug resistance and exploring medical applications. These findings suggest that conjugates could be explored for future therapies, serving as potent antibacterial agents against resistant bacterial strains. However, further research is imperative to better understand and to optimize drug design with human trials to address pressing healthcare challenges. However, the prelimi-

nary findings of the present research work can assist as a baseline for developing suitable antibacterial nanoformulations.

■ ASSOCIATED CONTENT

Data Availability Statement

The data sets generated during the current study are not publicly available but are available from the corresponding author on reasonable request.

■ AUTHOR INFORMATION

Corresponding Author

Sumera Javad – Dept. of Botany, Lahore College for Women University, Lahore 54000, Pakistan; orcid.org/0000-0002-4703-9610; Email: zif_4@yahoo.com

Authors

Nadia Ghaffar – Dept. of Botany, Lahore College for Women University, Lahore 54000, Pakistan

Anis Ali Shah – Dept. of Botany, Division of Science and Technology, University of Education, Lahore 54770, Pakistan

Saiqa Ilyas – Dept. of Biotechnology, Lahore College for Women University, Lahore 44444, Pakistan

Abeer Hashem – Botany and Microbiology Department, College of Science, King Saud University, Riyadh 11451, Saudi Arabia

Graciela Dolores Avila-Quezada – Facultad de Ciencias Agrotecnológicas, Universidad Autónoma de Chihuahua, 31350 Chihuahua, México

Elsayed Fathi Abd Allah – Plant Production Department, College of Food and Agricultural Sciences, King Saud University, Riyadh 11451, Saudi Arabia

Amina Tariq – Dept. of Botany, Lahore College for Women University, Lahore 54000, Pakistan

Complete contact information is available at: <https://pubs.acs.org/10.1021/acsomega.3c07000>

Author Contributions

Conceptualization: S.J. and A.A.S.; methodology, data collection, and original data analysis: N.G. and S.I.; data presentation and writing: N.G. and A.T.; reviewing and editing: A.H., G.D.A.-Q., and E.F.A.; and funding acquisition: A.H. and E.F.A. All authors have read and agreed to the published version of the manuscript.

Funding

The authors would like to extend their sincere appreciation to the Researchers Supporting Project Number (RSP2024R356), King Saud University, Riyadh, Saudi Arabia.

Notes

The authors declare no competing financial interest.

■ ACKNOWLEDGMENTS

The authors would like to extend their sincere appreciation to the Researchers Supporting Project Number (RSP2024R356), King Saud University, Riyadh, Saudi Arabia.

■ REFERENCES

- (1) Dye, C. After 2015: infectious diseases in a new era of health and development. *Philos. Trans. R. Soc., B* **2014**, *369*, No. 20130426.
- (2) Jamrozik, E.; Selgelid, M. J. Drug resistant Infection: Causes, Consequences, and Responses. In *Ethics and Drug Resistance: Collective Responsibility for Global Public Health*; Jamarozik, E.; Selgelid, M., Eds.; Springer Publishers, 2020.

- (3) Banerjee, S.; Kumari, V.; Shatabdi, D.; Moumita, D.; Arnab, G. Antibacterial, anti-biofilm activity and mechanism of action of pancreatin doped zinc oxide nanoparticles against methicillin-resistant *Staphylococcus aureus*. *Colloids Surf., A* **2020**, *190*, No. 110921.
- (4) Wang, N.; Xin, L.; Jingen, Li.; Qingfeng, Z.; Xiang, Li.; Qi, A. Antibacterial mechanism of the synergistic combination between streptomycin and alcohol extract from the *Chimonanthus salicifolius*. *J. Ethnopharmacol.* **2020**, *250*, No. 112467.
- (5) Luther, M. K.; Tristan, T. T.; Aisling, R. C.; David, D.; Thomas, P. L.; Kerry, L. L. Vancomycin Plus Piperacillin-Tazobactam and Acute Kidney Injury in Adults: A Systematic Review and Meta-Analysis. *Crit. Care Med.* **2018**, *46*, 12–20.
- (6) Gordon, J.; Lowy, F. D. Pathogenesis of methicillin-resistant *Staphylococcus aureus* infection. *Clin. Infect. Dis.* **2008**, *46*, 350–359.
- (7) Chambers, H. F.; Deleo, F. R. Waves of resistance: *Staphylococcus aureus* in the antibiotic era. *Nat. Rev. Microbiol.* **2009**, *7*, 629–641.
- (8) Becker, K. Methicillin-resistant *Staphylococcus aureus* and *Micrococci* at the interface of Human and animal health. *Toxins* **2021**, *13*, No. 61.
- (9) Tanomsridachchai, W.; Changkaew, K.; Changkawanyeeun, R.; Prapasawat, W. Antimicrobial resistance and molecular characterization of Methicillin-Resistant *Staphylococcus aureus* isolated from slaughter Pigs and pork in the central region of Thailand. *Antibiotics* **2021**, *10*, No. 206.
- (10) Fonkwo, P. N. Pricing infectious disease. The economic and health implications of infectious diseases. *EMBO Rep.* **2008**, *12*, S13–S17.
- (11) Fothergill, A. W. Antifungal Susceptibility Testing: Clinical Laboratory and Standards Institute (CLSI) Methods. In *Interactions of Yeasts, Moulds and Antifungal Agents*; Hall, G. S., Ed.; N. J. Humana Press: Totowa, 2012; pp 65–74.
- (12) Shruthi, T. S.; Meghana, M. R.; Medha, M. U.; Sajana, S.; Navya, P. N. Streptomycin fictionalization on silver nanoparticles for improved antibacterial activity. *Mater. Today: Proc.* **2019**, *10*, 8–15.
- (13) Pauksch, L.; Sonja, H.; Marcus, R.; Gabor, S.; Volker, A. Biocompatibility of silver nanoparticles and silver ions in primary human mesenchymal stem cells and osteoblasts. *Acta Biomater.* **2014**, *10*, 437–439.
- (14) Ling, D.; Hyeon, T. Chemical design of biocompatible iron oxide nanoparticles for medical applications. *IBS* **2013**, *7*, 1450–1466.
- (15) Parvekar, P.; Jayant, P.; Sandeep, M. Antibacterial efficacy of silver nanoparticles against *Staphylococcus aureus*. *Indian J. Nat. Sci.* **2020**, *10*, 0976–0997.
- (16) Yu, F.; Xuan, F.; Huimin, J.; Miaoxing, L.; Xiaotong, S.; Chaowen, X.; Tingtao, C.; Xiaolei, A.; et al. Zn or O? An atomic level comparison antibacterial activities of zinc oxides. *Chemistry* **2016**, *22*, 8053–8058.
- (17) Li, W. R.; Xiao, B. X.; Qing, S. S.; Shun, S. D.; You, S. O. Antibacterial effect of silver nanoparticles on *Staphylococcus aureus*. *Biometals* **2011**, *24*, 135–141.
- (18) Tran, Q. H.; Nguyen, V. Q.; Le, A. T. Silver nanoparticles: synthesis, properties, toxicology, applications, and perspectives. *Adv. Nat. Sci.: Nanosci. Nanotechnol.* **2013**, *4*, No. 033001.
- (19) Yousaf, H.; Ansar, M.; Khawaja, S. A.; Muhammad, R. Green synthesis of silver nanoparticles and their application as an alternative antibacterial and antioxidant agents. *Mater. Sci. Eng., C* **2020**, *112*, No. 110901.
- (20) Salem, S. S.; Fouda, A. Green synthesis of metallic nanoparticles and their prospective biotechnological applications: an overview. *Biol. Trace Elem. Res.* **2021**, *199*, 344–370.
- (21) Salem, S. S. Baker's yeast-mediated silver nanoparticles: Characterization and antimicrobial biogenic tool for suppressing pathogenic microbes. *BioNanoScience* **2022**, *12*, 1220–1229.
- (22) Soliman, M. K. Y.; Abu-Elghait, M.; Salem, S. S.; Azab, M. S. Multifunctional properties of silver and gold nanoparticles synthesis by *Fusarium pseudonygamai* Biomass *Convers. Biorefin.* **2022**.
- (23) Al-Rajhi, A. M. H.; Salem, S. S.; Alharbi, A. A.; Abdelghany, T. M. Ecofriendly synthesis of silver nanoparticles using Kei-apple (*Dovyalis caffra*) fruit and their efficacy against cancer cells and clinical

- pathogenic microorganisms. *Arabian J. Chem.* **2022**, *15* (7), No. 103927.
- (24) Mohsen, E.; Ola, M. I. B.; Mona, B.; Mohamed; Irens, S. F. Synthesis and characterization of ciprofloxacin loaded silver nanoparticles and investigation of their antibacterial effect. *J. Radiat. Res. Appl. Sci.* **2020**, *13*, 416–425.
- (25) Nishanthi, R.; Malathi, S.; John, P. S.; Palani, P. Green synthesis and characterization of bioinspired silver, gold, and platinum nanoparticles and evaluation of their synergistic antibacterial activity after combining with different classes of antibiotics. *Mater. Sci. Eng., C* **2019**, *96*, 693–707.
- (26) Elakraa, A. A.; Salem, S. S.; El Sayyad, G. S.; Attia, M. S. Cefotaxime incorporated bimetallic silver-selenium nanoparticles: Promising antimicrobial synergism, antibiofilm activity, and bacterial membrane leakage reaction mechanism. *RSC Adv.* **2022**, *12*, 26603–26619.
- (27) Ghaffar, N.; Sumera, J.; Muhammad, A. F.; Anis, A. S.; Mansour, K.; Gatasheh, B. M. A.; AlMunqedhi; Ozair, C. Metal nanoparticles assisted revival of streptomycin against MDRS *Staphylococcus aureus*. *PLoS One* **2022**, *17* (1–25), No. e0264588.
- (28) Soliman, M. K. Y.; Salem, S. S.; Abu-Elghait, M.; Azab, M. S. Biosynthesis of silver and gold nanoparticles and their efficacy towards antibacterial, antibiofilm, cytotoxicity, and antioxidant activities. *Appl. Biochem. Biotechnol.* **2023**, *195*, 1158–1183.
- (29) Selvaraj, V.; Suresh, S.; Lakshmipathy, M.; Mohd-Rafe, J.; Jiban, P. Eco-friendly approach in the synthesis of silver nanoparticles and evaluation of optical, surface morphological, and antimicrobial properties. *J. Nanostruct. Chem.* **2019**, *9*, 153–162.
- (30) Hawar, S. N.; Al-Shmgani, H. S.; Zainb, A.; Al-Kubaisi, G. M.; Sulaiman, Y. H. D.; Jesamine, J. R. Green Synthesis of Silver Nanoparticles from *Alhagi graecorum* Leaf Extract and Evaluation of Their Cytotoxicity and Antifungal Activity. *J. Nanomater.* **2022**, *2022*, No. 1058119.
- (31) Mengesha, Y. A. Phytochemical extraction and screening of bioactive compounds from black cumin (*Nigella sativa*) seeds extract. *Am. J. Life Sci.* **2015**, *3*, 358–364.
- (32) Hasan, K. N.; Yoke, H. C.; Perveen, N.; Paliwal, N. Phytochemical screening, antimicrobial and antioxidant activity determination of *Trigonella foenum-graecum* seeds. *Pharm. Pharmacol. Int. J.* **2019**, *7*, 321–343.
- (33) Ghaffar, N.; Javad, S.; Farrukh, M. A.; Shah, A. A.; Gatasheh, M. K.; AlMunqedhi, B. M. A.; Chaudhry, O. Metal nanoparticles assisted revival of streptomycin against MDRS *Staphylococcus aureus*. *PLoS One* **2022**, *17* (3), No. e0264588.
- (34) Harshinya, M.; Manickam, M.; Gangasalam, A.; Shanmugam, K.; Shanmuganathan, R. Enhancement of antibacterial properties of silver nanoparticles ceftriaxone conjugate through *Mukia maderaspatana* leaf extract mediated synthesis. *Ecotoxicol. Environ. Saf.* **2015**, *3*, 231–342.
- (35) Singh, P.; Mijakovic, I. Strong antimicrobial activity of silver nanoparticles obtained by the green synthesis in *Viridibacillus* sp. extracts. *Front. Microbiol.* **2022**, *13*, No. 820048.
- (36) Mahmood, S. J.; Azlan, A. A.; Dheyab, M. A. Green synthesis: Proposed mechanism and factors influencing the synthesis of platinum nanoparticles. *Green Process. Synth.* **2020**, *9*, 386–398.
- (37) Sharma, S.; Kumar, K.; Thakur, N. The effect of shape and size of ZnO nanoparticles on their antimicrobial and photocatalytic activities: A green approach. *Bull. Mater. Sci.* **2020**, *43*, No. 20.
- (38) Okaiyeto, K.; Ojemaye, M. O.; Hoppe, H.; Mabinya, L. V.; Okoh, A. I. Phyto fabrication of silver/silver chloride nanoparticles using aqueous leaf extract of *Oedera genitifolia*: Characterization and antibacterial potential. *Molecules* **2019**, *24*, No. 4382.
- (39) Oves, M.; Rauf, M. A.; Aslam, M.; Qari, H. A.; Sonbol, H.; Ahmad, I.; Zaman, G. S.; Saeed, M. Green synthesis of silver nanoparticles by *Conocarpus lancifolius* plant extract and their antimicrobial and anticancer activities. *Saudi J. Biol. Sci.* **2022**, *29*, 460–471.
- (40) Al-Aboody, M. S. Silver/silver chloride (Ag/AgCl) nanoparticles synthesized from *Azadirachta indica* latex and its antibiofilm activity against fluconazole-resistant *Candida tropicalis*. *Artif. Cells Nanomed. Biotechnol.* **2019**, *47*, 2107–2113.
- (41) Rautela, A.; Jyoti, R.; Mira, D. Green synthesis of silver nanoparticles from *Tectona grandis* seeds extract characterization and mechanism of antimicrobial action on different microorganisms. *J. Anal. Sci. Technol.* **2019**, *10*, No. 5.
- (42) Neel, S.; Mandal, A.; Dutta, A.; Saha, S.; Das, A.; Chawla, G.; Kundu, A. Response surface methodology guided process optimizations, modeling and biofunctional analysis of phytochemicals from *Nigella sativa* seeds as a potential antifungal agent. *Ind. Crops Prod.* **2023**, *199*, No. 116695.
- (43) Lakshmi, K. R.; Sri Venkata, N. P.; Girija, S. G.; Veerabhadra, S. P.; Venkata, R. M. K. A review on anti-bacterials to combat resistance: from ancient era of plants and metals to present and future perspectives of green nano technological combinations. *Asian J. Pharm. Sci.* **2019**, *7*, 42–59.
- (44) Filippi, A.; Mattiello, A.; Musetti, R.; Elisa, P.; Bradiot, E.; Marchiol, L. Green synthesis of Ag nanoparticles using plant metabolites. *AIP Conf. Proc.* **2017**, *1873*, No. 020004.
- (45) Selim, Y. A.; Maha, A.; Azb, I. R.; Mohamed, H. M. Green Synthesis of Zinc Oxide Nanoparticles Using Aqueous Extract of *Deverra tortuosa* and their Cytotoxic Activities. *Sci. Rep.* **2020**, *10*, No. 3445.
- (46) Singh, N. B.; Singh, A.; Hussain, I.; Singh, H.; Singh, S. C. Synthesis, characterization and application of ruthenium oxide nanoparticles on growth and metabolism of *Brassica oleracea* L. *Adv. Sci. Lett.* **2015**, *21*, 2635–2640.
- (47) Ahmad, W.; Divya, K. Green synthesis, characterization and antimicrobial activities of ZnO nanoparticles using *Euphorbia hirta* leaf extract. *J. King Saud Univ., Sci.* **2022**, *32*, 2358–2364.
- (48) Amutha, S.; Sridhar, S. Green synthesis of magnetic iron oxide nanoparticle using leaves of *Glycosmis mauritiana* and their antibacterial activity against human pathogens. *J. Innovations Pharm. Biol. Sci.* **2018**, *5*, 22–26.
- (49) de Alcântara Sica de Toledo, L.; Rosseto, H. C.; Bruschi, M. L. Iron oxide magnetic nanoparticles as antimicrobials for therapeutics. *Pharm. Dev. Technol.* **2018**, *23*, 316–323.
- (50) Sharma, P.; Pant, S.; Rai, S.; Yadav, R. B.; Dave, V. Green synthesis of silver nanoparticle capped with *Allium cepa* and their catalytic reduction of textile dyes: An ecofriendly approach. *J. Polym. Environ.* **2018**, *26*, 1795–1803.
- (51) Sathishkumar, P.; Preethi, J.; Vijayan, R.; Yusoff, A. R. M.; Ameen, F.; Suresh, S.; Balagurunathan, R.; Palvannan, T. Anti-acne, anti-dandruff and anti-breast cancer efficacy of green synthesized silver nanoparticles using *Coriandrum sativum* leaf extract. *J. Photochem. Photobiol., B* **2016**, *163*, 69–76.
- (52) Alkhatlan, A. H.; Hessah, A. A. A.; Mujeeb, K.; Merajuddin, K.; Abdullah, A.; Musaed, A.; Aws, A.; Hamad, Z. A.; Rafiq, M.; Siddiqui, V. Ecofriendly synthesis of silver nanoparticles using aqueous extracts of *Zingiber officinale* (ginger) and *Nigella sativa* L. seeds (black cumin) and comparison of their antibacterial potential. *Sustainability* **2020**, *12*, No. 10523.
- (53) Azizian-Shermeh, O.; Valizadeh, M.; Taherizadeh, M.; Beigomi, M. Phytochemical investigation and phytosynthesis of eco-friendly stable bioactive gold and silver nanoparticles using petal extract of saffron (*Crocus sativus* L.) and study of their antimicrobial activities. *Appl. Nanosci.* **2020**, *10*, 2907–2920.
- (54) Roy, N.; Mondal, S.; Laskar, R. A.; Basu, S.; Mandal, D.; Begum, N. A. Biogenic synthesis of Au and Ag nanoparticles by Indian propolis and its constituents. *Colloids Surf., B* **2010**, *76*, 317–325.
- (55) Hussein, E. A. M.; Mohammad, A. A. H.; Harraz, F. A.; Ahsan, M. F. Biologically synthesized silver nanoparticles for enhancing tetracycline activity against *Staphylococcus aureus* and *Klebsiella pneumoniae*. *Braz. Arch. Biol. Technol.* **2019**, *62*, No. 232.
- (56) Khorrami, S.; Zarrabi, A.; Khaleghi, M.; Danaei, M.; Mozafari, M. Selective cytotoxicity of green synthesized silver nanoparticles against the MCF-7 tumor cell line and their enhanced antioxidant and antimicrobial properties. *Int. J. Nanomed.* **2018**, *13*, 8013–8024.

- (57) Haider, A.; Ijaz, M.; Ali, S.; Haider, J.; Imarn, M.; Majeed, H.; Shazadi, L.; Ali, M. M.; Khan, J. A.; Ikram, M. Green synthesized phytochemically (*Zingiber officinale* and *Allium sativum*) reduced nickel oxide nanoparticles and confirmed bactericidal and catalytic potential. *Nanoscale Res. Lett.* **2020**, *15*, No. 50.
- (58) Kumar, N.; Das, S.; Jyoti, A.; Kaushik, S. Synergistic effect of silver nanoparticles with doxycycline against *Klebsiella pneumoniae*. *Int. J. Pharm. Pharm. Sci.* **2016**, *8*, 183–186.
- (59) Hsueh, Y. H.; Lin, K. S.; Ke, W. J.; Hsieh, C. T.; Chiang, C. L.; Tzou, D. Y.; Liu, S. T. The antimicrobial properties of silver nanoparticles in *Bacillus subtilis* are mediated by released Ag⁺ ions. *PLoS One* **2015**, *10*, No. e0144306.
- (60) Ali, M.; Muhammad, I.; Muhammad, I.; Anwar, Ul-H.; Muhammad, A.; Aftab, A. A. Biogenic synthesis, characterization and antibacterial potential evaluation of copper oxide nanoparticles against *Escherichia coli*. *Nanoscale Res. Lett.* **2020**, *16*, No. 148.
- (61) Fouda, A.; Hassan, S. E. D.; Saied, E.; Azab, M. S. An eco-friendly approach to textile and tannery wastewater treatment using maghemite nanoparticles (γ -Fe₂O₃ -NPs) fabricated by *Penicillium expansum* strain (K-w). *J. Environ. Chem. Eng.* **2021**, *9*, No. 104693.
- (62) Das, S. S.; Alkahtani, S.; Bharadwaj, P.; Ansari, M. T.; AlKahtani, M. D.; Pang, Z.; Hasnain, M. S.; Nayak, A. K.; Aminabhavi, T. Molecular insights and novel approaches for targeting tumor metastasis. *Int. J. Pharm.* **2020**, *585*, No. 119556.
- (63) Khan, M.; Al-Hamoud, K.; Liaquat, Z.; Shaik, M. R.; Adil, S. F.; Kuniyil, M.; Alkhatlan, H. Z.; Al-Warthan, A.; Siddiqui, M. R. H.; Mondeshki, M. Synthesis of Au, Ag, and Au–Ag bimetallic nanoparticles using *Pulicaria undulata* extract and their catalytic activity for the reduction of 4-nitrophenol. *Nanomaterials* **2020**, *10*, No. 1885.
- (64) Xia, T.; Kovochich, M.; Liong, M.; Madler, L.; Gilbert, B.; Shi, H. Comparison of the mechanism of toxicity of zinc oxide and cerium oxide nanoparticles based on dissolution and oxidative stress properties. *ACS Nano* **2008**, *2*, 2121–2134.
- (65) Khan, B.; Nawaz, M.; Hussain, R.; Price, G. J.; Warsi, M. F.; Waseem, M. Enhanced antibacterial activity of size-controlled silver and polyethylene glycol functionalized silver nanoparticles. *Chem. Pap.* **2021**, *75*, 743–752.
- (66) Ibraheem, D. R.; Hussein, N. N.; Sulaiman, G. M.; Mohammed, H. A.; Khan, R. A.; Rugaie, O. A. Ciprofloxacin-loaded silver nanoparticles as potent nano-antibiotics against resistant pathogenic bacteria. *Nanomaterials* **2022**, *12* (16), No. 1808.
- (67) Kalita, S.; Kandimalla, R.; Sharma, K. K.; Katak, A. C.; Deka, M.; Kotoky, J. Amoxicillin functionalized gold nanoparticles reverts MRSA resistance. *Mater. Sci. Eng., C* **2016**, *61*, 720–727.
- (68) Grace, A. N.; Pandian, K. Quinolone antibiotic-capped gold nanoparticles and their antibacterial efficacy against Gram-positive and Gram-negative organisms. *J. Bionanosci.* **2007**, *1*, 96–105.
- (69) Shaker, M. A.; Shaaban, M. I. Formulation of carbapenems loaded gold nanoparticles to combat multi-antibiotic bacterial resistance: In vitro antibacterial study. *Int. J. Pharm.* **2017**, *525*, 71–84.
- (70) Cui, Y.; Zhao, Y. Y.; Tian, Y.; Zhang, W.; Lu, X. Y.; Jiang, X. Y. The molecular mechanism of action of bactericidal gold nanoparticles on *Escherichia coli*. *Biomaterials* **2012**, *33*, 2327–2333.
- (71) Slomberg, D. L.; Lu, Y.; Broadnax, A. D.; Hunter, R. A.; Carpenter, A. W.; Schoenfisch, M. H. Role of size and shape on biofilm eradication for nitric oxide-releasing silica nanoparticles. *ACS Appl. Mater. Interfaces* **2013**, *5*, 9322–9329.
- (72) Cheon, J. Y.; Kim, S. J.; Rhee, Y. H.; Kwon, O. H.; Park, W. H. Shape-dependent antimicrobial activities of silver nanoparticles. *Int. J. Nanomed.* **2019**, *14*, 2773–2780.
- (73) Abbaszadegan, A.; Ghahramani, Y.; Gholami, A.; et al. The effect of charge at the surface of silver nanoparticles on antimicrobial activity against Gram-positive and Gram-negative bacteria: a preliminary study. *J. Nanomater.* **2015**, *2015*, No. 720654.
- (74) Rai, M.; Deshmukh, S.; Ingle, A.; Gade, A. Silver nanoparticles: the powerful nano weapon against multidrug-resistant bacteria. *J. Appl. Microbiol.* **2012**, *112*, 841–852.
- (75) Li, P.; Li, J.; Wu, C. Z.; Wu, Q. S.; Li, J. Synergistic antibacterial effects of beta-lactam antibiotic combined with silver nanoparticles. *Nanotechnology* **2005**, *16*, 1912–1917.
- (76) Duran, N.; Marcató, P. D.; Conti, R. D.; Alves, O. L.; Costa, F.; Brocchi, M. Potential use of silver nanoparticles on pathogenic bacteria, their toxicity and possible mechanisms of action. *J. Braz. Chem. Soc.* **2010**, *1*, 949–959.
- (77) Chopra, I. The increasing use of silver-based products as antimicrobial agents: a useful development or a cause for concern? *J. Antimicrob. Chemother.* **2007**, *59*, 587–590.
- (78) Allahverdiyev, A. M.; Kon, K. W.; Abamor, E. S.; Bagirova, M.; Rafailovich, M. Coping with antibiotic resistance: combining nanoparticles with antibiotics and other antimicrobial agents. *Expert Rev. Anti-Infect. Ther.* **2011**, *9*, 1035–1052.
- (79) Roshmi, K. R.; Soumya, M.; Jyothis, E. K.; Radha, K. Effect of biofabricated gold nanoparticle-based antibiotic conjugates on the minimum inhibitory concentration of bacterial isolates of clinical origin. *Gold Bull.* **2015**, *48*, 63–71.
- (80) Magalhaes, N. S.; Mosqueira, V. C. F. Nanotechnology applied to the treatment of malaria. *Adv. Drug Delivery Rev.* **2010**, *62*, 560–575.
- (81) Zhang, Y. W.; Peng, H. S.; Huang, W.; Zhou, Y. F.; Yan, D. Y. Facile preparation and characterization of highly antimicrobial colloidal Ag or Au nanoparticles. *J. Colloid Interface Sci.* **2008**, *325*, 371–376.
- (82) Kamal, R.; Razzaq, A.; Shah, K. A.; Khan, Z. U.; Khan, N. U.; Mena, F.; Iqbal, H.; Cui, J. Evaluation of cephalexin-loaded PHBV nanofibers for MRSA-infected diabetic foot ulcers treatment. *J. Drug Delivery Sci. Technol.* **2022**, *71*, No. 103349.